Investigation of Thermo-acoustic Oscillations in a Trapped Vortex Model Combustor

P. Xavier[1,*], A. Vandel[1], G. Godard[1], B. Renou[1], G. Cabot[1], F. Grisch[1], M.A. Boukhalfa[1], M. Cazalens[2]

[1] CORIA UMR 6614 - Normandie University,
CNRS - University & INSA of Rouen,
Saint Etienne du Rouvray, 76800, France

[2] Safran R&T,
Rond Point Rene Ravaud,
Moissy Cramayel, 77550, France

Abstract

Self-sustained combustion instabilities in a trapped vortex model combustor (TVC) were experimentally investigated with high-speed laser diagnostics. We used particle image velocimetry (PIV) and OH-planar laser induced fluorescence (OH-PLIF) to record simultaneous measurements of the flow unsteadiness and the flame structure. Results showed the existence of an aerodynamic instability referred to as "jet flapping", and strongly disturbing the interfacial shear layer. A spatial analysis of velocity time traces confirmed that this instability was accounting for more than 80% of the total turbulent kinetic energy. This flow instability, combined with thermal expansion of burned gases, induced a flow rate modulation, modified the local equivalence ratio, and therefore weakened the flame stabilization process.

Introduction

Growing environmental concerns have led to significant restrictions concerning permissible pollutant emissions of aircraft gas turbines (GT). Lean premixed (LP) combustion is one promising solution [1] but results in severe phenomena, such that risks of flashback, flame blow-off at partial load regimes, and combustion instabilities induced by thermo-acoustic oscillations [2–4].

A possible solution to prevent these undesired phenomena consists in integrating cavity flame holders in the combustion chamber to improve flame stabilization. This concept has been extensively investigated in scramjet hypersonic combustors [5]. Investigation for subsonic applications, known as the trapped vortex combustor (TVC), have been investigated since the early 1990s. The TVC concept can be assimilated to a staged combustor, operating with the well known rich-burn/rich-quick/lean-burn combustion regime. In fact, it uses a recirculating rich flow trapped in a cavity to create a recirculating zones of hot combustion products. Their rapid mixing with a lean main mixture passing above the cavity provides a continuous ignition source and stabilize the flame [6, 7]. One of the main advantage of this technology lies on the natural confinement of the rich zone, which acts as the primary stabilization source. In comparison with advanced swirl-stabilized combustors, many studies demonstrated enhanced performance levels regarding LBO limits, altitude relight, and pollutant emissions [6–10].

However, this combustor raises major issues for the design and the range of stable operating conditions. In fact, the coupling between the natural flow unsteadiness [11, 12] and the heat release rate can lead to the appearance of thermo-acoustic oscillations. Burguburu et al. [13] and Xavier et al. [14] recorded numerous stable operating conditions in the present TVC but they also highlighted the existence of acoustically unstable operating conditions. Remarkably, few studies focused on these restrictive conditions [9, 15] and provide good reasons to understand effects on flame stabilization.

The aim of the present work was to experimentally investigate effects of thermo-acoustic oscillations on the flow dynamics and flame stabilization efficiency. For this reason, we voluntary operated the TVC in conditions presenting large-amplitude pressure oscillations (i.e., p'_{rms} = 1430 Pa) and we took advantage of high-speed optical diagnostics. The paper is organized as follows: first, the experimental setup, test conditions, and diagnostics are described. Second, A temporal analysis of one combustion instability cycle is provided prior to investigating pressure-flow-flame dynamics. Finally, we analyze effects of acoustics on the flow field and its effects on the combustion process.

Experiments

1. *Trapped Vortex Combustor and Operating conditions*

Experiments were conducted in a fully annular transparent TVC model combustor, depicted in Fig. 1. The burner was inserted into a Herasil cylindrical quartz tube with an inner diameter of 80 mm and a length of 200 mm. This quartz tube was surrounded by a second protective transparent casing equipped with planar quartz windows. An adaptive nozzle, located at the burner outlet was used to set the absolute pressure P_{glob} of the combustor to 0.17 MPa. Additional details can be found in [16].

The cavity region is shown in Fig. 1 (b). The mainstream flow consisted of a mixture of air and methane (CH_4) with a nominal air mass flow rate $\dot{m}^o_m$ of 21.54

*Corresponding author: pradip.xavier@coria.fr

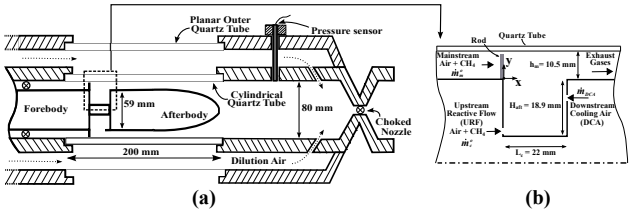

Figure 1: (a) Schematic representation of the experimental setup. $\bigotimes$: choked nozzle. (b) Details of the cavity region in the TVC (L_c = 22 mm, H_{aft} = 18.5 mm). The origin for measurements is located at the cavity leading edge.

$g.s^{-1}$ (bulk velocity of 5.0 $m.s^{-1}$) and a resulting equivalence ratio ϕ_m of 0.8. It flowed in a 10.5 mm high annular gap created between the forebody and the cylindrical quartz tube. Acting as flame holders, 20 rods, each with a diameter of 3 mm, were positioned on the upstream cavity corner, and produced a blockage area of 23% in the mainstream. Two injector systems were located inside the cavity. The upstream reactive flow (URF) injection system delivered a mixture of air and CH_4 with a nominal air mass flow rate $\dot{m}_c^o$ of 0.70 $g.s^{-1}$ (bulk air velocity of 6.0 $m.s^{-1}$) and an equivalence ratio ϕ_c of 3.0. This injection system was installed in the lower part of the upstream cavity face by means of a 1 mm annular slot. The downstream cooling air (DCA) injection system generated a nominal air mass flow rate $\dot{m}_{DCA}$ of 1.0 $g.s^{-1}$ (bulk air velocity of 3.6 $m.s^{-1}$). The DCA system was placed 8 mm below the downstream cavity edge by means of a 1 mm annular slot. The global equivalence ratio in the burner ϕ_{glob} was 0.83 and the nominal power of the TVC was 60 kW, of which 83% were produced by the main flame and the remaining 17% were produced by the cavity pilot flame. Table 1 summarizes operating conditions investigated in the present study and selected from previous preliminary studies [13, 16]. Note that the pressure fluctuation amplitude for this unstable condition was measured at p'_{rms} = 1430 Pa. Moreover, to prevent any external acoustic contributions, the inlet and outlet boundary conditions were choked using adaptive nozzles.

	Main	URF	DCA
Flow rate [g.s^{-1}]	22.54	0.82	1.0
Bulk velocity [m.s^{-1}]	5.0	6.0	3.6
ϕ [-]	0.8	3.0	0.0
fuel [g.s^{-1}]	1.0	0.12	0.0
Power [kW]	50	10	0
$P_{glob}[MPa]$		0.17	

Table 1: TVC operating conditions.

2. *Diagnostics*

a. *10kHz OH-PLIF system*

A high-speed OH-PLIF system operating at a repetition rate of 10kHz was used to study flame dynamics and to record the hydroxyl radical (OH) in the flame. A 10 kHz Nd-YAG-laser (EdgeWave IS2011-E) operating at 532nm with an average power of 100W was used to pump a tunable dye laser (Sirah Credo) supplied with Rhodamine 590 dye. The frequency-doubled pulse energy was 460μJ/shot and the resultant energy was 130μJ/shot in the probe volume. The excitation wavelength was tuned to the $Q_1(5)$ ro-vibronic transition of the $A^2\Sigma^+(\nu' = 0) \leftarrow X^2\Pi(\nu'' = 1)$ band (λ =282.75nm). The resultant laser beam was overlapped with the PIV beam by using a dichroic mirror and was expanded through a set of fused silica lenses (f_1 = 1000mm, f_2 = -20mm) to form a laser sheet of 30 mm in height (Fig. 2). The detection system consisted of an external image intensifier (HighSpeed IRO, LaVision) connected to a CMOS-camera (Fastcam SA1) with a resolution of 512x512 pix^2 (21.5 pix/mm magnification ratio). The UV lens (100mm f/2 B-Halle Nachfl. GmbH) was mounted on a Scheimpflug system because the camera was titled at a 15° angle (away from the laser sheet normal) due to the central metal body and the presence of the PIV camera. The intensifier gate was set to 500 ns, and background noise arising from elastic scattering of the particles used for PIV was reduced with a high-pass colored optical filter (Schott WG305). We adopted a broadband collection strategy from 308 to 330 nm with a band-pass colored filter (Schott UG11). Spatial inhomogeneity of the laser sheet profile was taken into account and corrected by filling the combustion chamber with a mixture of acetone vapor and air. The optical distortion caused by the oblique viewing angle and the curved face of the quartz tube was systematically corrected prior to performing the experiments.

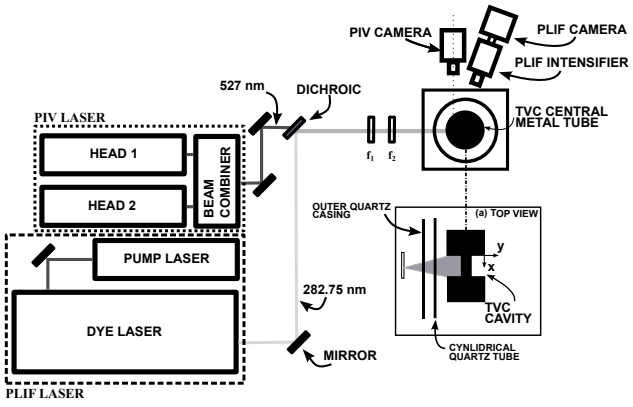

Figure 2: Schematic representation of the dual measurement technique.

b. *2.5kHz PIV system*

A high-speed PIV system operating at a repetition rate of 2.5kHz was used to study flow dynamics. The repetition rate resulted in a compromise imposed by the spatial resolution of the camera used in this study. A double cavity Nd:YLF laser (Darwin Dual, Quantronix) operating at 527nm fired two laser beams, 15 μs apart (each cavity was operating at 2.5kHz). The laser beams were trans-

mitted and combined with the UV laser beam through the dichroic mirror and expanded through the same lenses used for the PLIF beam. We used ZrO_2 particles to seed the various flow injection conditions (generated by means of several fluidized beds). Light scattering was collected on a 5kHz high-speed CMOS-camera (Phantom V10) equipped with a Nikon f/2.8 105mm lens. The camera was set to a resolution of 480x480 pix^2, resulting in a 24 pixel/mm magnification ratio. PIV image processing was performed with a multi-pass interrogation window algorithm (DynamicStudio, Dantec) resulting in a final interrogation window of 32x32 pix^2 and a 50% overlap. A coherent filter was finally applied to correct isolated false vectors.

c. *Additional measurement techniques*

A dynamic pressure sensor (Kistler 7061B ThermoComp®, 10 kHz sampling rate) was mounted on a waveguide system, 280 mm downstream from the cavity region (Fig. 1(a)). Spatial offset was taken into account by applying a temporal correction, considering that the shift occurred mainly because of a propagating acoustic wave [17]. We used one-sided power spectral density (PSD) with the Welch method for the acoustic mode detection [18]. Results are given as sound pressure levels (SPL, units in $dB.Hz^{-1}$) with a frequency resolution of $\pm$ 5 Hz. Temporal fluctuations in the heat release were collected on a 10 kHz sampling rate photo multiplier tube (PMT, Hamamatsu 6780-20) with a selected photocathode of 0.15nA low dark current. The output signal of the PMT was amplified with a Hamamatsu C7319 pre-amplifier (10^6 gain). A BG12 band-pass optical filter was used to record spontaneous CH* emission, thus providing a good estimator for the heat release oscillations [19, 20].

Results and Discussions

1. *Description of combustion instabilities*

We present in this section a temporal sequence along one combustion instability cycle in order to demonstrate effects of thermo-acoustic oscillations on the flow field and flame structure. Figure 3 depicts a sequence of instantaneous OH-PLIF and PIV measurements corresponding to the operating conditions presented in Tab. 1. The figure illustrates instantaneous coupling of velocity vector fields colored by their corresponding magnitudes and locations of burned gases (OH signal in greyscale). The corresponding pressure and CH* values are given in the graph on the right in Fig. 3 (numbered red dots). The region of interest relative to the entire burner is given in the upper right schema. The axial and radial velocity components u and v are also defined.

When the unsteady pressure was null and the unsteady heat release was at maximum (Fig. 3 #1), the flow located in the downstream part of the cavity was radially ejected towards the main channel. Although this flow behavior was decreasing, it continued to be observed, as depicted in Fig. 3 #2. This ejection process

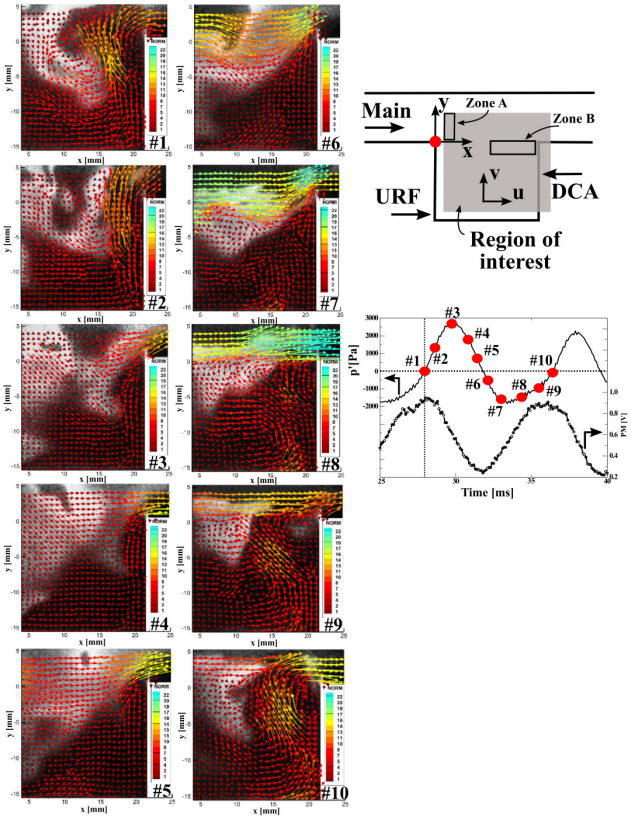

Figure 3: Simultaneous OH traces and velocity measurements (colored according to magnitude) for an individual pressure cycle.

had a tremendous effect: It blocked the mainstream flow and created a region of low velocities. Burned gas locations were also altered by this ejection process. The three subsequent snapshots (Fig. 3 #3, #4, and #5) highlight a totally different behavior. In fact, the ejection process disappeared when pressure and heat release decreased. Velocities in the cavity were relatively low, without any preponderant flow topology. In contrast, the axial mainstream velocity u was constantly increasing. Snapshots #6, #7, and #8 were taken when the heat release started to increase; they clearly show that the main channel flowed without being blocked. Consequently, burned gases located above the cavity were drained towards the exhaust line so that few traces were found in this region. Simultaneously, several vortices and recirculation zones appeared in the developing flow in the cavity. At this point, burned gases were well established in the shear layer at the interface between the main channel and the cavity. With continually increasing pressure (snapshot #8, #9, and #10), the ejection process, which started to penetrate the main flow, became apparent and the cycle was over.

We conclude from this sequence that an intense flow instability greatly modified the flow, the heat release rate, and location of burned and unburned gases. The absence of periodic vortex shedding processes also demonstrated

that jet injections inside the cavity modified the conventional mechanism of vortex-flame interactions observed in backward-facing step or dump combustors [21, 22]. Instead, this instability, referred to as *jet flapping,* and which alternated between the cavity and the main channel was preponderant and could negatively affect the flame stabilization.

2. *Flow field dynamics*

In order to assess to what extent the flow dynamics was affected by acoustics and if it existed one or several characteristic flow structures which could be related to these thermo-acoustic oscillations, we used the proper orthogonal decomposition (POD) approach [23–25]. The main idea of the classical POD technique is to decompose a velocity field $u(\mathbf{x}, t)$ as

$$u(\mathbf{x}, t) \approx \sum_{k=1}^{K} a_k(t)\Phi_k(\mathbf{x}), \qquad (1)$$

where $\mathbf{x}$ is a vector containing the velocity components, $\Phi_k(\mathbf{x})$ are space functions, $a_k(t)$ are time coefficients, and K is a positive integer used to approximate the variable of interest $u(\mathbf{x}, t)$.
The normalized energy of the 10 first POD modes revealed that most of the energy was contained in the first mode, with 73% of the total turbulent kinetic energy (whatever the axial or radial velocity component). Therefore, we considered only the first mode to reconstruct a low-order flow field encountered in the TVC.

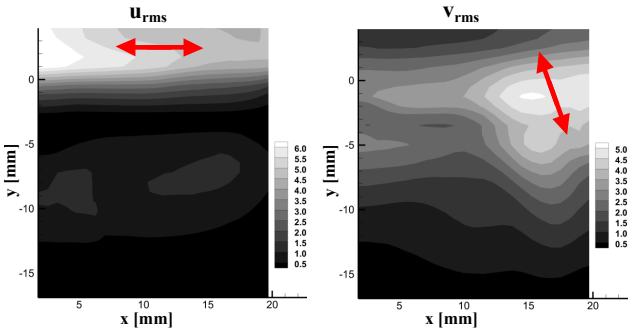

Figure 4: Root mean square (RMS) velocity component fields, calculated from the first POD mode. Left: u_{rms}. Right: v_{rms}

The root mean square of (RMS) each velocity fluctuation component is shown in Fig. 4. The first mode shows that axial fluctuations were quite important in the mainstream. This flow behavior was associated to the alternate *jet flapping* penetration and the resulting mainstream blockage. The latter process was also visible next to the cavity trailing edge and confirms that the mutual interaction between these two flows was driving the instability. We definitively conclude that the *jet flapping* mechanism was the only preponderant mechanism driving the flow dynamics and then thermo-acoustic oscillations.

3. *Mass transfers and flame stabilization*

Consequences of the *jet flapping* on the flame stabilization were therefore investigated. Mass transfers between the cavity and the mainstream may affect and deteriorate the flame stability. We then considered the two zones presented in Fig. 3 and we extracted instantaneous velocity components as well as the instantaneous gas composition[†]. The latter was estimated by calculating the spatial averaged progress variable $< c >$, being zero in unburned gases and unity in burned gases [26]. Results are given in Fig. 5 and show two probability density functions (pdfs), which were estimated with 5000 data. It shows the probablity to encounter a pair of ($< c >$,u) values. Note that the axial velocity component was considered in zone A whereas the radial velocity component was considered in zone B.

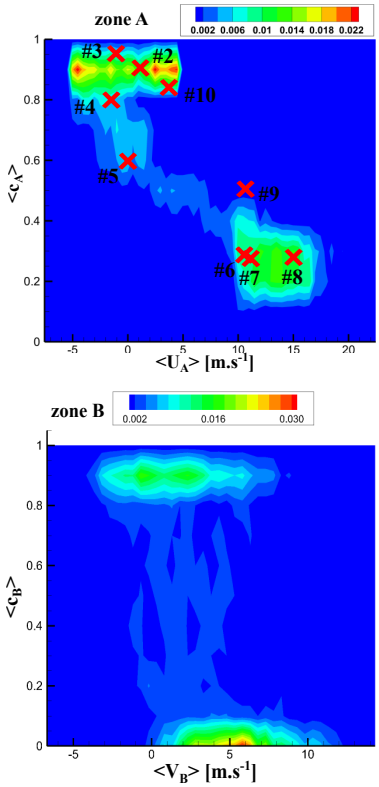

Figure 5: Probability density functions (pdfs) of the spatially averaged progress variables with the corresponding averaged velocity component. 5000 instantaneous data were considered. Top: pdf in zone A with the averaged axial velocity. Bottom: pdf in zone B with the averaged radial velocity.

The pdf on the top presents a bimodal distribution, with a segregation between $< c_A >$ = 1 and $< c_A >$ = 0.25. When the mainstream was ignited ($< c_A >$ = 1), axial velocities were quite low, revealing the cavity blockage, primarily due to the *jet flapping*. When the mainstream was flowing normally (i.e., high axial velocities), $< c_A >$ values were reduced to $< \bar{c}_A >$ $\approx$ 0.25 and proves that the main flow was draining burned gases and that no flame was present above the cavity. The pdf of the zone B (Fig. 5 bottom) presents a similar bimodal distribution. When $< c_B >$ = 0 (i.e.,

[†]Data extracted from these zones were spatially averaged with the operator $< \cdot >$.

unburned gases), the radial velocity was increased and is clearly representative of the *jet flapping*. Thus, gases drained with the *jet flapping* consisted most of the time in unburned gases. Moreover, low radial velocity were associated to values of $< c_B >$ almost close to unity.

We placed several instantaneous data on the pdf in zone A (top) in order to understand the combustion dynamics along one cycle of instability. These data correspond to red crosses and numbering is identical to Fig. 3. It is clearly visible that the burner was operating alternately between the two spikes of the pdf, with a defined path. We can therefore conclude that great differences in both velocities and gas composition affected the flame stabilization and led to an unstable feature.

Conclusion

A trapped vortex combustor exhibiting self-sustained pressure oscillations was experimentally investigated in order to assess the main mechanisms piloting the instability. Thermo-acoustic oscillations induced a large-scale coherent: a large interaction between the cavity and the mainstream was found to be the primary source for the unsteady flow dynamics. Consequences of this coherent mechanism were important: large and inefficient mass transfers between the cavity and the mainstream. In particular, composition of the exchanged gases alternated between completely burned and unburned gases, which finally led to a pulsed combustion regime and weakened the flame stabilization.

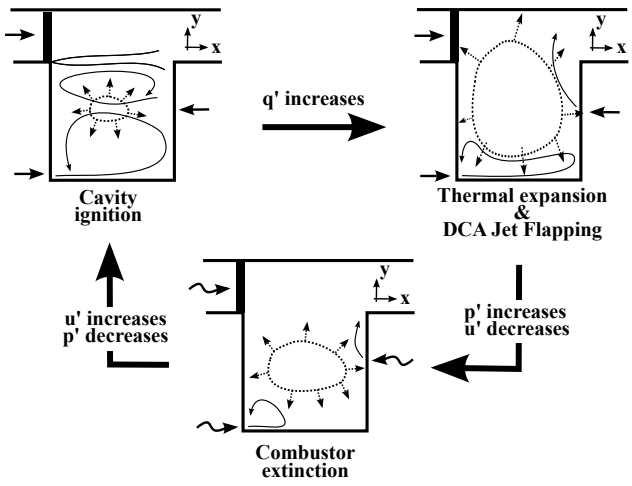

Figure 6: Schematic illustration of the mechanism of combustion instabilities encountered in the present TVC.

Figure 6 presents the mechanism that best explains the present data set:

- First, cavity jet injections circulated normally and efficient mixing enabled the cavity to ignite. At this moment, the DCA jet injection was injected into the cavity and the heat release was constantly increasing.
- Second, the cavity ignition became violent, mainly due to the cavity confinement and thermal gas expansion. Consequently, the DCA jet was deflected towards the mainstream and annihilating the flow topology.
- Third, in parallel to the *jet flapping* aerodynamic instability, we suppose that the pressure increase may induce a flow rate oscillation, which in turn may disturb both cavity and mainstream flow dynamics and cause the burner extinction.
- Fourth, the cavity flow dynamics started to establish as the heat release was at minimum and the cycle was over.

Balance of the aerodynamics between the cavity and the main channel could be a critical parameter in order to spatially locate the mixing region produce a stable recirculation zone for an efficient flame stabilization. Investigation of alternative cavity injection systems will also be subject to future work in order to optimize the whole geometry.

Acknowledgements

The research leading to these results has received funding from the European Community's Seventh Framework Programme (FP7/2007-2013) under Grant Agreement n° ACP0-GA-2011-265586.

References

[1] A. WULFF, J. HOURMOUZIADIS, Aerospace Science and Technology 8 (1997) 557–572.

[2] P. GOKULAKRISHNAN, M. RAMOTOWSKI, G. GAINES, C. FULLER, R. JOKLIK, L. ESKIN, M. KLASSEN, R. ROBY, Journal of engineering for gas turbines and power 130 (2008) 051501.

[3] T. LIEUWEN, V. McDONNELL, E. PETERSEN, D. SANTAVICCA, Journal of engineering for gas turbines and power 130 (2008) 11506.

[4] S. CANDEL, Proceedings of the Combustion Institute 29 (2002) 1–28.

[5] A. BEN-YAKAR, R. HANSON, Journal of Propulsion and Power 17 (2001) 869–877.

[6] K. HSU, L. GOSS, D. TRUMP, W. ROQUEMORE, Journal of Propulsion and Power 14 (1998) 57–65.

[7] K. HSU, L. GROSS, D. TRUMP, W. ROQUEMORE, in: 33rd AIAA Aerospace Sciences Meeting and Exhibit, Reno, NV, USA, pp. 95–0810.

[8] V. R. KATTA, W. ROQUEMORE, Journal of engineering for gas turbines and power 120 (1998) 60–68.

[9] W. ROQUEMORE, D.SHOUSE, D. BURNS, A. JOHNSON, C. COOPER, B. DUNCAN, K. HSU, V. KATTA, G. STURGESS, I. VIHINEN, in: 39th AIAA Aerospace Sciences Meeting and Exhibit, Reno, NV, USA, pp. 2001–0489.

[10] D. BURRUS, A. JOHNSON, W. ROQUEMORE, D. SHOUSE, in: ASME Tubo Expo 2001, Atlanta, USA, pp. GT2001–0087.

[11] G. BROWN, A. ROSHKO, Journal of Fluid Mechanics 64 (1974) 775–816.

[12] L. N. CATTAFESTA, Q. SONG, D. R. WILLIAMS, C. ROWLEY, F. ALVI, Progress in Aerospace Sciences 44 (2008) 479–502.

[13] J. BURGUBURU, G. CABOT, B. RENOU, A. BOUKHALFA, M. CAZALENS, in: Proceedings of the ASME, Copenhagen, Denmark, pp. GT2012–68451.

[14] P. XAVIER, A. VANDEL, G. GODARD, F. GRISCH, B. RENOU, G. CABOT, M. BOUKHALFA, M. CAZALENS, in: Proceedings of the ASME, Dusseldorf, Germany, pp. GT2014–25207.

[15] K. HSU, C. CARTER, V. KATTA, W. ROQUEMORE, in: 37th AIAA Aerospace Sciences Meeting and Exhibit, Reno, NV, USA, pp. 99–0488.

[16] P. XAVIER, G. CABOT, B. RENOU, A. BOUKHALFA, M. CAZALENS, in: Proceedings of the ASME, San Antonio, USA, pp. GT2013–94704.

[17] C. MERLIN, Simulation numérique de la combustion turbulente: Méthode de frontières immergées pour les écoulements compressibles, application à la combustion en aval d'une cavité, Ph.D. thesis, INSA Rouen, France, 2012.

[18] P. WELCH, volume 15, IEEE Transactions on Audio and Electroacoustics, pp. 70–73.

[19] H. NAJM, P. PAUL, C. MUELLER, P. WYCKOFF, Combustion and Flame 113 (1998) 312–332.

[20] R. PRICE, I. HURLE, T. SUGDEN, Proceedings of the Combustion Institute 12 (1969) 1093–1102.

[21] A. GHONIEM, S. PARK, A. WACHSMAN, A. ANNASWAMY, D. WEE, H. M. ALTAY, Proceedings of the Combustion Institute 30 (2005) 1783–1790.

[22] H. ALTAY, R. SPETH, D. HUDGINS, A.F.GHONIEM, Combustion and Flame 156 (2009) 1111–1125.

[23] J. LUMLEY, Atmospheric turbulence and radio wave propagation 64 (1967) 166–178.

[24] G. BERKOOZ, P. HOLMES, J. LUMLEY, Annual review of fluid mechanics 25 (1993) 539–575.

[25] L. CORDIER, M. BERGMANN, in: Lecture series 2002-04 on post-processing of experimental and numerical data, Von Karman Institute for Fluid dynamics.

[26] T. CHEW, R. BRITTER, K. BRAY, Combustion and Flame 75 (1989) 165–174.